Research Article

Research on the Bionic Flexible End-Effector Based on Tomato Harvesting

Tiezheng Guo [iD],[1] **Yifeng Zheng** [iD],[1,2] **Weixi Bo** [iD],[1] **Jun Liu,**[2] **Jie Pi,**[2] **Wei Chen,**[1] **and Junzhuo Deng** [iD][1]

[1]*Industrial Center, Nanjing Institute of Technology, Nanjing 211167, China*
[2]*Institute of Agricultural Facilities and Equipment, Jiangsu Academy of Agricultural Sciences, Key Laboratory of Protected Agriculture Engineering in the Middle and Lower Reaches of Yangtze River, Ministry of Agriculture, Nanjing 210014, China*

Correspondence should be addressed to Tiezheng Guo; guotiezheng@njit.edu.cn

Aiming at the problems that tomatoes are fragile and the traditional end-effector design is not suitable for tomato picking, a combination of the bionic principle of FRE structure and finger design was proposed. Based on the physical properties of tomatoes, a flexible underactuated end-effector for tomato picking and sorting was designed. The optimal structural parameters of fingers were determined by finite element analysis, and the tomato grasping experiment was carried out. The results show that the flexible end can grasp and transport tomatoes with diameters ranging from 65 to 95 mm without damage, which can withstand 7 N tensile force, the load is more than 2 times of its own weight, the tomato coverage rate is greater than 23.6%, and the effective grab rate is 100% and has the advantages of the strong stability, universality, and protection. The research provides a novel solution for the design and application of the tomato picking and sorting robot end-effector.

1. Introduction

Tomato is an important vegetable crop, with a total annual output of 177 million tons and a planting area of about 5 million hectares [1]. China has the huge amount of cultivation and consumption of tomatoes, with an area of 1.109 million hectares and an annual yield of 64.832 million tons [2]. In the entire tomato production chain, the picking and sorting period are the most time-consuming and laborious part. Its labor demand accounts for more than 50% of the entire planting and production process. Until now, it has been mostly done manually, and has met the problems such as expensive labor, low efficiency, and large workload [3]. In recent years, tomato harvesting robots have become the new trend with the visual recognition and intelligent control technology development and progress [4]. The end-effector, as the terminal component of the picking and sorting robot interacting with tomato, has a significant impact on the robot's work efficiency, fruit damage rate, and other operational performance. It has become one of the key technolo-

gies in the research and development of tomato harvesting robots.

The picking and sorting end-effectors have developed so far can be divided into two categories: rigid end-effectors and flexible end-effectors. Rigid end-effector, as the most commonly used agricultural harvesting end-effector, started early in research and had achieved many results. It is widely used in the harvesting of apples, citrus, sweet peppers, and other fruits and vegetables [5–7] and has the advantages of high precision requirements, fast response speed, and large grasping force. Naoshi Kondo's team at Kyoto University has developed a rigid end-effector for picking tomato clusters [8]. Its large size makes it difficult to carry out actual picking operations, and the picking success rate is only around 50%. Kochi University in Japan has developed a tomato thermal cutting actuator [9], which used resistance wire to cut the stalk. However, the cutting method has the certain security risks. Hiroaki Yaguchi's team at the University of Tokyo designed a three-finger rigid gripper. Due to the too large opening of the jaw design, multiple tomatoes

were caught or blocked by tomato vines, resulting in a successful picking rate of only 62.2% [10].

In contrast to traditional rigid end-effectors, the finger portion of the flexible end-effector is made of stretchable material. The material itself has good adaptability. It obtains infinite degrees of freedom by continuously deforming as it interacts with the object, replacing rigid joints and links. It has obvious advantages when grasping soft, fragile, or irregular objects. Structural deformation of flexible materials can be achieved in various ways, such as vacuuming the filling bag using the particle blocking principle [11, 12], changing the temperature to induce deformation of the shape memory material [13, 14], and inflating and deflating the elastic chamber [15, 16]. However, these flexible ends are limited to certain scenarios. Due to the small grasping force, if it is applied to fruit and vegetable picking and sorting, further research is required.

To sum up, most end-effectors are prone to damage the fruit during the working process or are not suitable for fruit picking and sorting in realistic scenarios. It will seriously affect the quality and storage time of the fruit and ultimately reduce the market price and economic benefits. The main reason is that the factors considered in the design of the end-effector are not comprehensive, resulting in unreasonable design. Therefore, in view of the crispness and particularity of tomato, a flexible underactuated end-effector suitable for tomato picking and sorting was designed based on the bionic principle of FRE (Fin Ray Effect) structure in this paper. Based on the experiment of tomato physical properties, the flexible finger structure was designed and optimized, and the finite element simulation analysis of finger force was completed. In order to provide the novel solution for the design and application of tomato picking and sorting robot end-effector, an experimental platform was built to conduct clamping experiments on the flexible end-effector, and the economy, reliability, and repeatability of the end-effectors were verified.

2. Physical Properties of Tomatoes

In order to make the designed flexible end-effector more suitable for tomatoes picking and sorting, research on the physical properties of tomatoes was carried out. The experiments included tomato geometry, mass, compression, and damage characteristics. The experimental subjects are Provence tomato varieties.

2.1. Research Methods

2.1.1. Tomato Geometry and Quality Tests. The flexible finger structure design is influenced by the size and weight of the tomato. Experimental site is greenhouse tomato planting base of Jiangsu Academy of Agricultural Sciences and experiment time May 6, 2022. A total of 5 rows of Provencal tomatoes were grown in the greenhouse. There were 10 plants in each row, and each plant had about 2 to 3 tomato clusters. 2 ripe tomatoes were randomly picked from each tomato plant, for a total number of 100. 57 tomatoes were randomly selected from 100 tomatoes, numbered 1 to 57.

A vernier caliper was used to measure the lateral diameter L_1, longitudinal diameter L_2 and height L_3 of the lateral diameter of the tomato. The specific measurement positions are shown in Figure 1. The mass m of tomato was measured with an electronic balance JA5001.

2.1.2. Compression Mechanical Properties Test. When the tomato is grasped by flexible fingers, the pulp of the tomato is squeezed, and the middle part of the tomato is the least compressive [17]. In order to study the compressive resistance of the middle position of the tomato, the compressive mechanical properties test was carried out on the tomatoes. The 57 tomatoes were divided into 19 groups, of which 18 were the experimental group and 1 group was the control group. The experiments were carried out using a TMS-TOUCH texture analyzer (FTC, USA). The test platform is shown in Figure 2(a). In the loading test, the test mode of the texture analyzer was selected as "Measure Force in Compression" mode. The running program was selected as "Return to Start" mode [18]. The test parameters are set as follows: the probe type of the instrument is a flat probe with a diameter of 50 mm. The probe and stage is covered with a layer of spacer made of TPU material, and the thickness of the material spacer is 1 mm. The probe loading speed is 30 mm/min, which belongs to the quasi-static range [19]. The speed before and after the test set to 60 mm/min. The initial distance between the probe and the stage is 110 mm, which is guaranteed to exceed the maximum transverse diameter of the tomato. Put the tomato longitudinally on the stage, and the probe is loaded with the maximum transverse diameter of the tomato, as shown in Figure 2(b). The loading displacement of the tomatoes was set to 1~18 mm, and they were divided into 18 groups, and each group was tested with 3 tomatoes.

2.1.3. Damage Characteristic Tests. Nondestructive gripping of tomato is an important research factor in the end-effector design process. Mechanical damage to tomatoes takes two forms. In the first, the tomato peel is not broken, but the cell structure is destroyed. The compressed part of the tomato undergoes an enzymatic reaction and darkens the color. The respiration of tomato cells is accelerated, and the compressed position loses a lot of water and contracts. Another type of damage is the rupture of the tomato peel, the exposure of the internal tissue, and the appearance of mildew on the surface of the tomato [20]. After passing the compression characteristic test, the tomatoes were damaged to varying degrees. Placed tomatoes on a lab bench labeled 0~18 mm and stored at room temperature in the lab. Wrinkling or molding of tomatoes with different loadings was recorded over 15 days.

2.2. Analysis of Physical Properties of Tomatoes

2.2.1. Size and Quality of Tomatoes. The measurement results of 57 tomatoes showed that the lateral diameter L_1 of the tomatoes ranged from 66.4 to 92.7 mm, the longitudinal diameter L_2 ranged from 52.6 to 81.3 mm, the lateral diameter and height L_3 ranged from 35.1 to 62.7 mm, and the tomato mass ranged from 152.7 to 378.2 g. The test
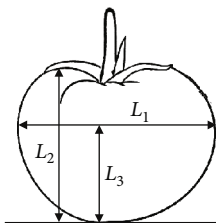
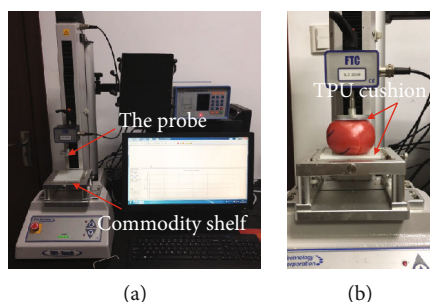Figure 1: Schematic diagram of tomato size measurement.

Figure 2: Compression mechanical properties experiment: (a) the composition of the texture analyzer; (b) loading experiment of tomato.

Table 1: Classification results of tomato geometry and quality.

Size/ (mm)	Proportion (%)	Maximum mass/(g)	Maximum transverse diameter height/ (mm)
65~70	3.5%	179.3	38.8
70~75	8.8%	210.6	42.7
75~80	43.9%	290.4	45.8
80~85	36.8%	305.2	50.5
85~90	5.2%	370.7	58.4
90~95	1.8%	400.4	62.7

results by size are shown in Table 1. In an ideal gripping state, the fingertips of the flexible fingers need to exceed the height of the maximum transverse diameter of the tomato, and the opening diameter of the finger end should be larger than the maximum transverse diameter of the tomato. Therefore, the length of the finger structure should be greater than 65 mm, and the maximum opening diameter of the finger should be greater than 95 mm.

2.2.2. Compression Mechanical Properties of Tomatoes. In the compressive mechanical properties test, the experimental results of the loading displacement of 18 mm are shown in Figure 3. The tomato compression process is divided into three stages: elastic compression stage, damage stage, and rupture stage. The loading force curve of tomato initially show an S-shaped curve. When the pressure exceeds the maximum elastic compression threshold of the tomato, the curve oscillates, and the pressure drops rapidly. Then it enters the stage of tomato damage, and the pressure gradually increases. After reaching the maximum, the tomato enters the burst stage, and the pressure drops again. The elastic compression stage is the range where the loading displacement is less than 10.5 mm in the figure. The damage stage is in the range of loading displacement of $10.5 < d < 16.5$ mm, and the tomato is obviously deformed at this stage. When the rupture stage is reached, the tomato cracks, and the maximum value of the pressure in the curve is the rupture force of the tomato.

After 18 groups of experiments, it was found that most of the tomatoes had obvious cracks in the experimental groups with a loading displacement of more than 11 mm. In the experimental group with a loading displacement of more than 5 mm, most of the tomatoes showed obvious

indentation. Therefore, the clamping force of the flexible fingers should be less than 30 N to ensure that the tomato will not be obviously damaged in appearance.

2.2.3. Damage Characteristics of Tomatoes. The 18 groups of tomatoes after the compression mechanical property test were used as experimental samples, and the uncompressed tomatoes were used as control samples, which were stored at room temperature for 15 days to observe the storage conditions of tomatoes. For tomatoes under pressure of about 30 N, no damage to the tomatoes can be observed, and there is no obvious indentation. But over time, the stressed skin of the tomatoes wrinkled and lost water. The storage results are shown in Table 2. With the increase of compressive force and compressive displacement, the storage time of tomatoes gradually shortened. When the compressive displacement is less than 2 mm, and the compressive force is less than 8 N, the storage time of tomatoes is more than 14 days. When the tomato compression displacement exceeds 5 mm, the storage time has decreased significantly. When the compression displacement is greater than 10 mm, the tomato has no storage conditions. Therefore, in order to achieve nondestructive picking of tomatoes, the clamping force of flexible fingers should be at least less than 8 N to ensure the longest storage time of tomatoes.

3. Structure Design and Optimization of Flexible End-Effector

3.1. Principles of Bionics. The FRE structure is inspired by the biological phenomenon of fish fins. When one side of the fin is pushed by the hand, the fin does not bend in the direction of the force but in the opposite direction [21]. Compared with the most widely used pneumatic fingers, the finger structure based on the fin ray effect principle does not require complicated air source control. The FRE structure allows compliant wrapping of objects by passively deforming upon contact with the target object without any external actuation. Following the FRE principle, the geometry of the finger is determined as a triangle consisting of two inclined fins fixed at one end and ribs evenly distributed in the middle. As shown in Figure 4, the fingers are broken down into three main modules: the base module, the middle module, and the fingertip module. The base module is mounted on a rigid fixed assembly that provides support for the closed chain structure as well as the entire finger

element. The middle module consists of a rib-like structure that provides mechanical properties for the fingers, and the number can be extended to n. The fingertip module consists of a triangular structure.

In the existing research, some end-effectors equipped with such fingers have realized the adaptive grasping function for fruits of various shapes [22, 23]. However, after putting it into the tomatoes harvesting experiment, there are two problems to be solved. On the one hand, the finger design is overall longer to accommodate the most fruit sizes. When used to grasp the tomato, the finger does not completely wrap the tomatoes. On the other hand, the fins and rib structures of the fingers are designed to be thicker, resulting in a smaller amount of deformation of the fingers when they come into contact with the tomatoes. The load applied to the tomatoes was not buffered and was an indirect trigger for impaired tomato gripping. The advantage of the layer blocking effect of this type of finger structure is not exploited. Aiming at the above two problems, the key parameters such as the number and inclination of ribs of this type of fingers are deeply studied.

3.2. Mathematical Modeling of Single Finger. To better understand the kinematics of fingers, a closed-chain structural mathematical model is established. Fingers for mathematical modeling consist of a base module, two intermediate modules, and a fingertip module. Based on the closed-chain finger structure shown in Figure 5(a), the state vector of the system is as follows:

$$\boldsymbol{\gamma} = [a, k_1, k_2, k_3, k_4, k_5, k_6, k_7, k_8, \alpha_1, \alpha_2, \alpha_3]^T, \quad (1)$$

where $k_i (i \in \{1, \cdots, 8\})$ are the curvature of the flexible link, a is the stroke of the fixed joint, and $\alpha_j (j \in \{1, 2, 3\})$ are the angle of the rotating joint:

$$\theta_1 = \frac{\pi}{2} + L_1 k_1 + \alpha_1,$$

$$\theta_2 = \frac{\pi}{2} + L_1 k_1 + L_2 k_2 + \alpha_2, \quad (2)$$

$$\theta_3 = \frac{\pi}{2} + L_1 k_1 + L_2 k_2 + L_3 k_3 + \alpha_3,$$

where $L_m (m \in \{1,2,3\})$ is the curved length of the flexible link. $\theta_n (n \in \{1,2,3\})$ is the angle between the flexible link and the rib.

3.2.1. Forward Kinematics. To establish a closed-chain positive kinematics model, it is necessary to determine the constraint equations between joint variables and motion variables. The finger structure has 12 joint variables and 8 constraints, which are defined as follows:

$$\overline{AB} + \overline{BC} + \overline{CI} + \overline{IJ} + \overline{JA} = \lambda_1(a, k_1, \alpha_1, k_8) = 0, \quad (3)$$

$$\overline{CD} + \overline{DH} + \overline{HI} + \overline{IC} = \lambda_2(\alpha_1, k_2, \alpha_2, k_7) = 0, \quad (4)$$

$$\overline{DE} + \overline{EG} + \overline{GH} + \overline{HD} = \lambda_3(\alpha_2, k_3, \alpha_3, k_6) = 0, \quad (5)$$

$$\overline{EF} + \overline{FG} + \overline{GE} = \lambda_4(\alpha_3, k_4, k_5) = 0. \quad (6)$$

Determining the four joint variables in equation (1) as closed-chain system inputs, equations (3)–(6) can be used to solve for the remaining joint variables.

The analysis of a single flexible link is shown in Figure 5(b). When the fixed link is vertical (initial angle $\alpha = 0$), the position of point A in the Cartesian plane (x, y) is

$$A_x(\beta = 0) = R - R \cos\left(\frac{L}{R}\right) = \frac{1 - \cos(Lk)}{k},$$

$$A_y(\beta = 0) = R \sin\left(\frac{L}{R}\right) = \frac{\sin(Lk)}{k}, \quad (7)$$

where R is the radius of curvature $(R = 1/k)$ and L is the arc length of the flexible link. If β increases, the position of the connecting rod tip is

$$\begin{bmatrix} A_x \\ A_y \\ 0 \end{bmatrix} = \mathbf{R}_z(\beta) \begin{bmatrix} \dfrac{1 - \cos(Lk)}{k} \\ \dfrac{\sin(Lk)}{k} \\ 0 \end{bmatrix}$$

$$= \begin{bmatrix} \cos(\beta) \dfrac{1 - \cos(LK)}{K} - \sin(\beta) \dfrac{\sin(LK)}{K} \\ \sin(\beta) \dfrac{\sin(LK)}{K} + \cos(\beta) \dfrac{1 - \cos(LK)}{K} \\ 0 \end{bmatrix}. \quad (8)$$

Equation (8) and the standard kinematics are defined above, and the function λ_1, λ_2, λ_3, and λ_4 in equations (3)–(6) can be calculated.

3.2.2. Inverse Kinematics. In addition to constraint equations (3)–(6), the inverse kinematics of the closed chain employs additional constraints ($\overline{AF}$ and θ) given by the position and orientation of the fingertip points, expressed by equations (9) and (10). Choose an input variable from equation (1) to solve equations (3)–(6), (9) and (10).

$$\overline{AB} + \overline{BC} + \overline{CD} + \overline{DE} + \overline{EF} - \overline{AF} = \lambda_5(a, k_1, k_2, k_3, k_4) = 0, \quad (9)$$

$$\beta + L_1 k_1 + L_2 k_2 + L_3 k_3 + L_4 k_4 = \theta. \quad (10)$$

3.3. Design of Flexible Finger Structure. The finger structure was improved according to the experimental results of tomato physical properties to minimize the initial contact force when the finger interacted with the tomato (before the layer interference) and generate a relatively large clamping force after grasping the tomato (after the layer interference) while maintaining the dexterity needed for the fingers to passively adapt to the tomato shape.
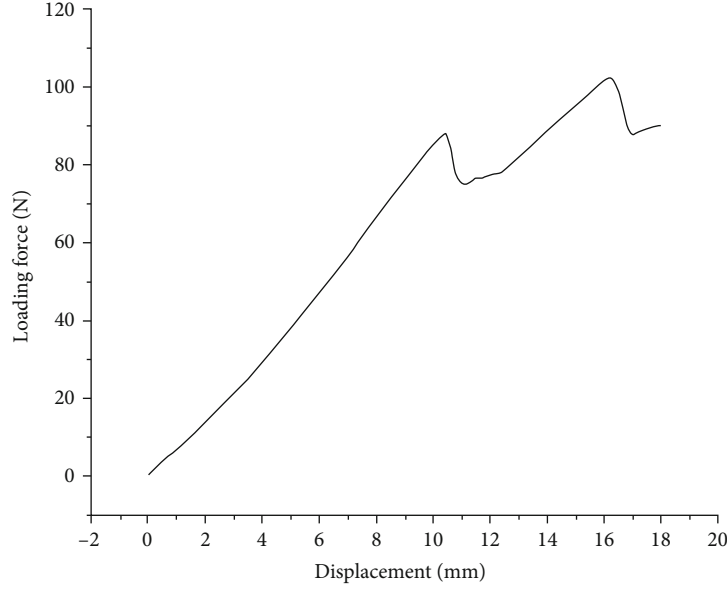
Figure 3: Pressure-displacement curve of tomato.

Table 2: Experimental results of damage characteristics.

Compression displacement/(mm)	Maximum compression force/(N)	Average storage days/(day)
0	0	15
1	5.56	14
2	8.03	14
3	13.42	12
4	15.28	10
5	27.15	8
6	35.78	7
7	43.56	5
8	40.03	6
9	57.09	4
10	68.57	3
11	80.89	2
12	82.71	1
13	87.36	0
14	90.12	1
15	90.69	1
16	101.23	0
17	112.33	0
18	110.79	0

Figure 4: Finger structure diagram: (a) no load state; (b) load state.

As shown in Figure 6, the finger is made of TPU material, and the basic structure remains unchanged. Set the fin length h to 70 mm to ensure that the fingertip position exceeds the maximum transverse diameter height when the finger is grasping the tomato, which solves the problem of excessive opening at the end. The base width is set to 36 mm to fit the finger fixing base. The thickness m of the fins in contact with the tomato is reduced to 1.5 mm, which ensures that the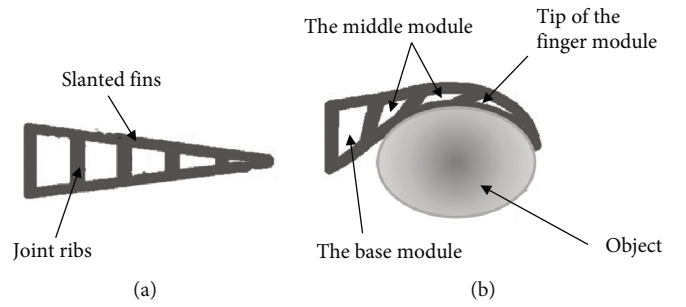 fingers are easily deformed when interacting with the tomato, and the initial contact force is minimized. At the same time, in view of the problem that the root position of the noncontact fin is prone to structural damage, the thickness n of the noncontact fin is set to 3 mm. Aiming at the problem of smooth surface of tomato, the contact fin surface is designed with different characteristic structures to increase the friction force and reduce the sliding during grasping. By changing the number of ribs, rib thickness t, inter-rib width e, and rib inclination angle θ, the relationship between the rib distribution law based on the layer blocking principle and the finger grip strength is further weighed.

First, determine the optimal number of ribs inside the finger, which is helpful for subsequent tests of rib thickness and angle changes. Secondly, the influence of fin structure changes on finger deformation is studied. By changing the rib thickness t, the effect of the rib thickness on the displacement of the fingertip was evaluated, and the most suitable rib size was selected. By changing the initial rib angle θ, the intercostal layer blocking effect during finger deformation is improved. Make the contact force between the finger and the tomato to the best state (when the θ changes, the rib width e will be adjusted appropriately).
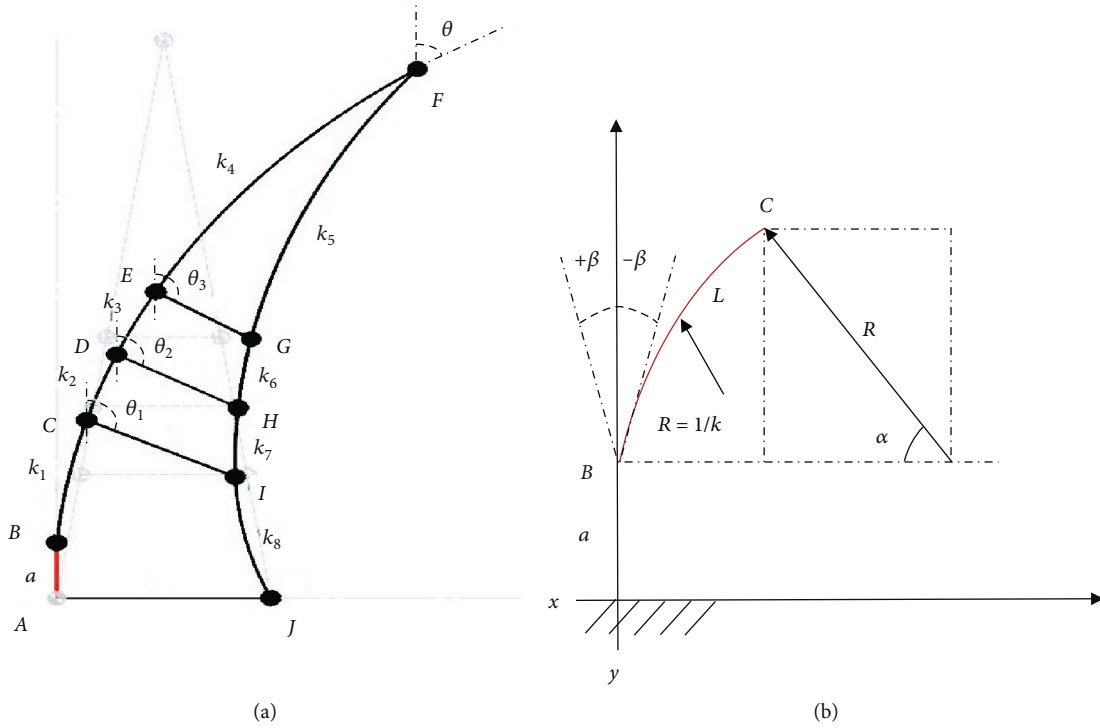
(a)

(b)

FIGURE 5: Mathematical model: (a) the composition of the single-finger structure; (b) single constant curvature section.
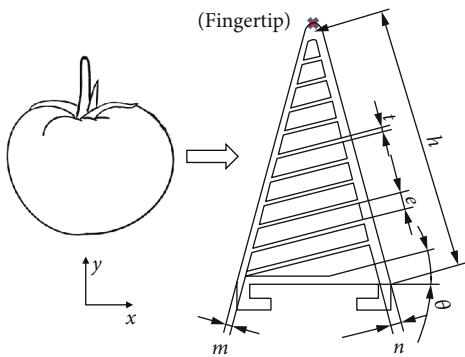

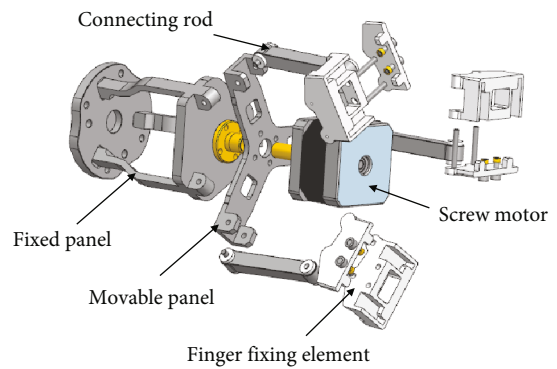FIGURE 6: Key design parameters of new flexible finger.

FIGURE 7: Design of fixed components.

3.4. Design of Fixed Components. Some progress has been made in the design method of the end-effector fixed components, but the rationality of the design still needs to be improved. For example, in the end structure design of reference [24], the screw motor passes through the fixed plate vertically upward and drives the slider to move up and down along the z-axis direction. However, the protruding lead screw takes up some of the space for the end-effector to grab the fruit. If the distance to the tomato is not properly controlled during the picking task, the rigid screw will come into contact with the crispy tomato on the surface, causing damage to the skin.

Therefore, based on the previous research experience, the structure of the end-effector is redesigned. The optimized fixing assembly consists of the finger fixing element, the support base, and the screw motor. Its structural exploded diagram is shown in Figure 7. The finger fixing element is fixed in cooperation with the flexible finger bottom structure. The support base is composed of a fixed panel, a movable panel and three connecting rods. The fixed panel is used to assemble the screw motor and support the rotation of the finger fixing element. In order to realize the rotational movement of the finger fixing element, the movable panel moves in coordination with the screw motor through the coupling. The two ends of the connecting rods are, respectively, connected in rotation with the movable panel part and the finger fixing element to drive the fingers to open and close. The support base can be connected with the robotic arm through accessories such as flanges.
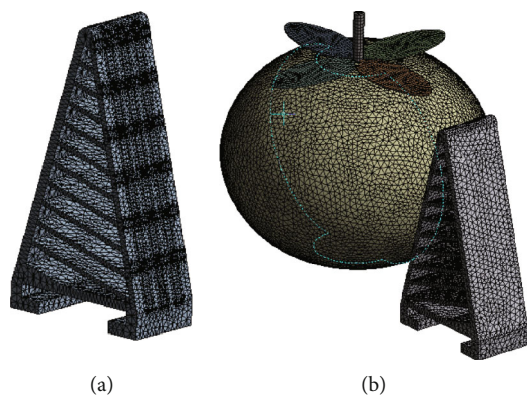
| | (a) | (b) |

FIGURE 8: Network model of tomato and fingers: (a) single-finger network diagram; (b) network diagram of tomato and finger assembly.

TABLE 3: Simulation results of fingers with different numbers of ribs.

Number of fins	Total deformation (mm)		
	5 N	10 N	15 N
6	8.896	Fracture	Fracture
8	7.223	12.748	Fracture
10	6.795	10.831	14.346

4. Finite Element Simulation

TPU material has the advantages of high tension and tensile force, but its deformation is difficult to predict due to the nonlinear factors of geometry and materials. Therefore, the finite element analysis software ANSYS (ANSYS 2020 R2) is used to simulate the static structure of fingers and tomato to analyze the bending performance. The key parameters of the TPU material are set as follows: Shore hardness = 85 A, density = 1200 kg/m^3, Young's modulus = 11.7 MPa, and Poisson's ratio = 0.45 [25]. Create a Static Structural module in ANSYS Workbench, add TPU material properties, and enter the parameters to get the model. Take one of the fingers as an example, determine the mesh accuracy of the finger, and use tetrahedral elements to divide the model, as shown in Figure 8. Set the element size to 1 mm, and the fingers are divided into 74942 nodes and 41455 elements.

4.1. Analysis of Single-Finger Force

4.1.1. Change in the Number of Ribs.
The number of ribs inside the finger was set to 6, 8, and 10; the rib angle θ was uniformly set to 0°; and loads of 5, 10, and 15 N were applied to the finger surface, respectively. When a tomato is in contact with a finger, the initial contact area is about 60 square centimeters. The stress area is selected in the middle of the finger, 20 unit surfaces are selected horizontally, and 3 unit surfaces are selected vertically, which are consistent with the actual contact area to the greatest extent. The simulation results are shown in Table 3. When a finger with 6 ribs is subjected to a load of 5 N, the total deformation of the finger is about 8.896 mm, which shows better extensibility than other fingers. But broken phenomenon appeared when subjected to 10 and 15 N loads. Fingers with 8 ribs can withstand loads of 5 and 10 N but break down when subjected to a load of 15 N. It is proved that the rigidity of these two finger structures is insufficient. The fingers with 10 ribs have a certain degree of stretchability while ensuring the load conditions. Therefore, it is more appropriate to set 10 ribs inside the finger.

4.1.2. Rib Thickness Variation.
The influence of the thickness of the rib on the overall stiffness of the finger is analyzed. Set the fin thickness t to 0.6, 1.2, 1.8 mm, which is an integer multiple of the nozzle diameter of the 3D printer to ensure smooth printing. The rib angle θ is uniformly set to 0° to control the variable. A load force of 10 N was applied to the finger surface to obtain the tip displacements in the x and y directions of the finger for different rib thicknesses. As shown in Figure 9(a), when a load of 10 N is applied, the fingertip with a 1.8 mm rib thickness is displaced 11.2 mm along the x-axis, while the finger with a 0.6 mm rib thickness has only a displacement of 4.5 mm. The less tip travel on the x-axis indicates that the fingertip displacement is absorbed by the internal structure of the finger and the more passively adaptive the finger is. As shown in Figure 9(b), the fingertip with 1.8 mm rib thickness is displaced 5.3 mm along the y-axis direction, while the 0.6 mm rib tip is displaced by 8.7 mm. It is proved that the thinner the rib, the greater the deformation of the middle of the finger structure along the x-axis and the greater the travel of the fingertip along the y-axis. To sum up, the finger structure with 0.6 mm rib thickness is more in line with the design principles and requirements.

4.1.3. Rib Inclination Variation.
Increasing the rib inclination can reduce the initial contact force of the fingers. The maximum contact force was increased by the layer blocking effect. Set the rib thickness to 0.6 mm, the number of ribs to 10, and the rib inclination angle θ to be 0~60° in increments of 10°. A 10 N load was applied to the finger surface, and the layer blocking effect and the maximum displacement of the finger structure with different rib inclination angles were analyzed. The simulation effect is shown in Figure 10. When the rib inclination angle is 10° and 20°, the ribs do not appear to fit each other, and the difference in the maximum displacement of the finger deformation is small. When the inclination angle of the rib reaches 30°, the finger exhibits a layer blocking effect, and the maximum displacement decreases significantly.

As shown in Figure 11, as the inclination angle of the rib increases, the maximum displacement of the finger deformation fluctuates up and down. When the rib inclination angle is 30°, the layer blocking effect is obvious, and the displacement reaches the minimum. When the inclination angle continues to increase, the maximum displacement shows
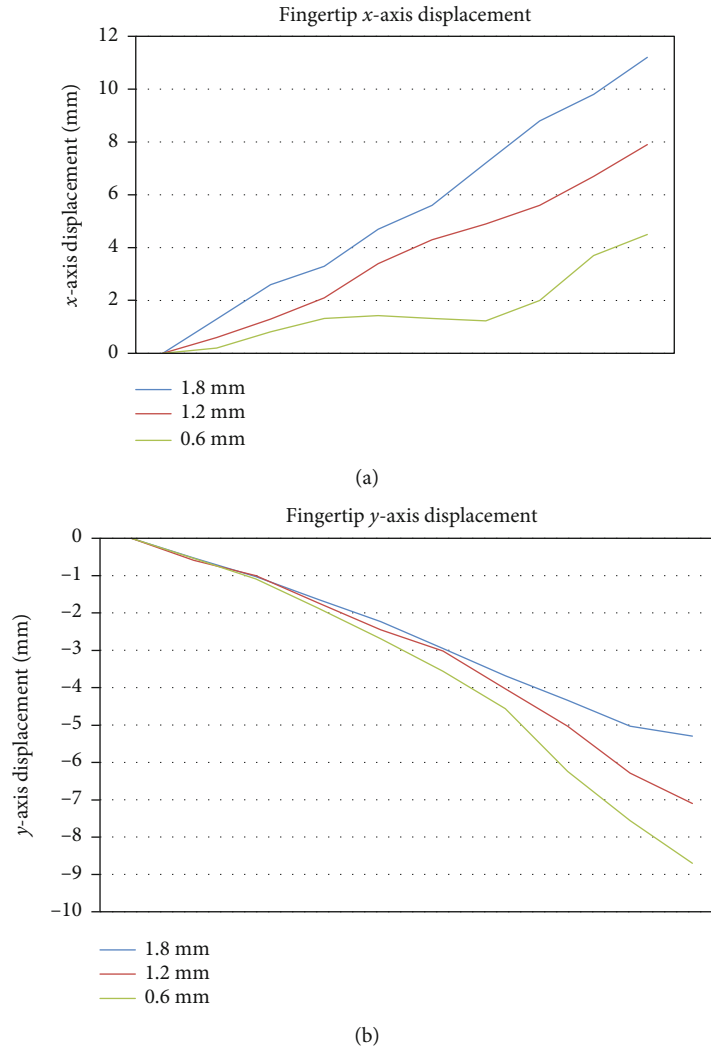
Fingertip *x*-axis displacement

(a)

Fingertip *y*-axis displacement

(b)

FIGURE 9: Simulation of fingertip displacement: (a) *x*-axis displacement; (b) *y*-axis displacement.

an upward trend again. It shows that the excessive dip angle has an adverse effect on the layer blocking effect. Therefore, the finger structure produces the best layer blocking effect at a rib inclination angle of 30°.

4.2. Simulation of Single-Finger Interaction with Tomato. The tomato is set as a fixed support, and the contact area between the finger and the tomato is set as frictionless contact. The interaction force is set to 10 N, the large deflection setting in the solver is turned on, and the total deformation is solved. The simulation results are shown in Figure 12. After comparing the total deformation of the finger and the displacement of the fingertip in the *x* and *y* directions with the single-finger analysis above, it is found that the data error is within ±0.2 mm, which verifies the accuracy of the data and conclusions.

In summary, through the analysis of the simulation results, the optimized finger structure parameters are obtained: the number of ribs is 10, the rib thickness is 0.6 mm, and the rib inclination angle is 30°.

5. Experimental Verification

5.1. Fabrication of the End-Effector. The finger structure of TPU material and the finger holder of resin material were printed with the standard FDM printer X-max. The rest of the panels are made of aluminum alloys. The total mass of the end-effector is 464.7 g. As shown in Figure 13, an Arduino Mega 2560 microcontroller is used as the control core, and a two-phase four-wire stepper motor is used to power the end-effector. The thin film pressure sensor is fixed on the surface of the finger to detect and record the force of each grasping tomato.

5.2. Single-Finger Experiment

5.2.1. Experiments on Finger Surface Features. The surface of the tomato is smooth. In order to avoid sliding during grasping, three structures with different surface features were designed on the contact surface of the flexible fingers to increase the friction force, numbered 1 to 3, as shown in Figure 14(a). An experimental platform was built to test
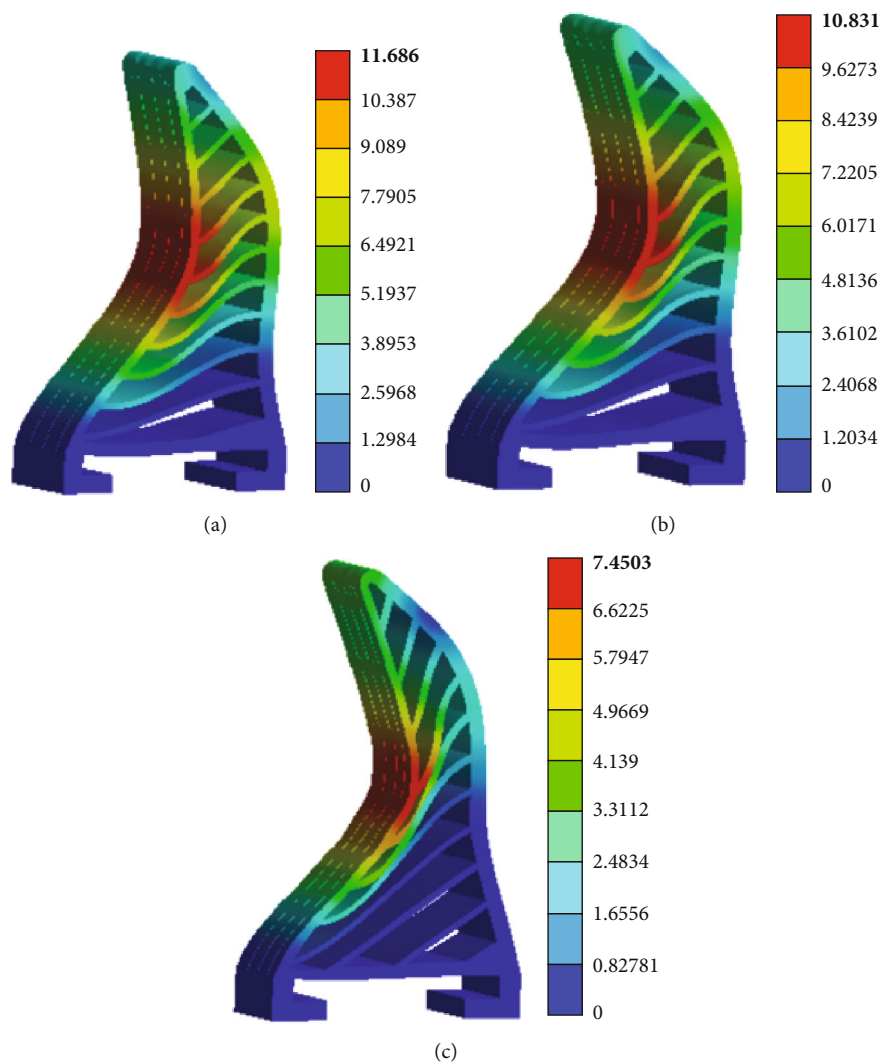
FIGURE 10: Layer blocking effect simulation of fingers: (a) 10° inclination; (b) 20° inclination; (c) 30° inclination.
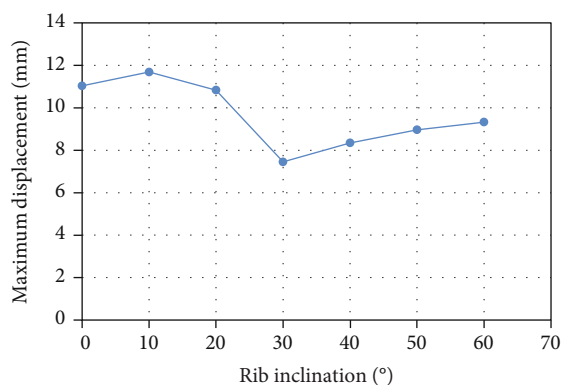

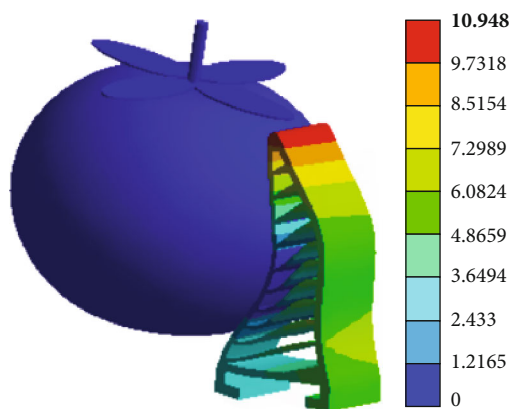FIGURE 11: Relationship between maximum displacement and rib inclination.

FIGURE 12: Simulation of tomato and finger interaction.

the frictional force generated when different surface features interact with tomatoes. As shown in Figure 14(b), the three surface feature structures were made into thin surfaces with an area of 10×15 cm and fixed on the test bench. Place the tomato on a thin surface and connect the dynamometer to the tomato through a string, so that it is on the same level as the tomato. The tension meter moves at a uniform speed
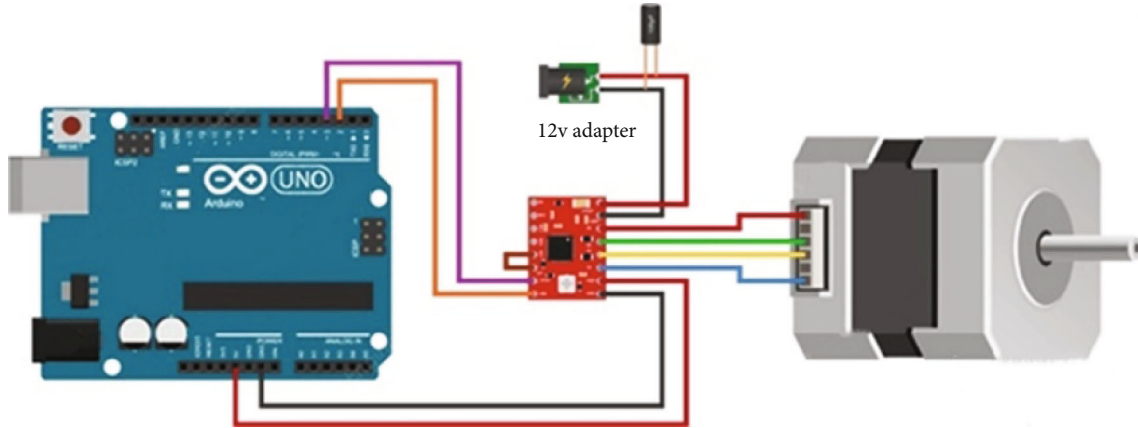
FIGURE 13: Control system of end-effector.

1.51N	1.45N	1.67N	1.39N
1	2	3	4

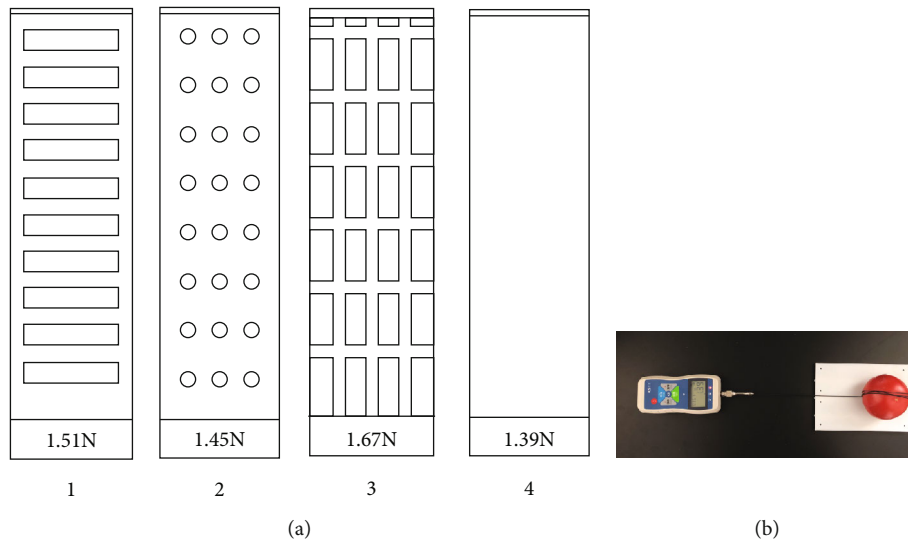(a)   (b)

FIGURE 14: Friction test: (a) structure of different surface features; (b) experimental device.

along a straight line, pulling the tomato to displace until the tomato moves away from the thin surface. Record the maximum pulling force during this process. The experiment was repeated 10 times for each structure and averaged. Compared to the smooth surface structure (No. 4), the surface with the characteristic structure produces better friction effect. Comparing different surface feature structures, the No. 3 grid is selected as the finger surface feature structure.

5.2.2. Experiment on Finger Deformation. The finger load experiment was carried out to analyze the deformation of four typical finger structures under 10 N pressure. The bottom of the finger is fixed in a vise, and a load of 10 N is applied to the middle of the surface of the finger fin using a tension gauge. The position before and after the force is recorded at the position, and the displacement is calculated. As shown in Figure 15, the six-rib finger structure suffered structural damage under 10 N pressure. The 10-rib finger structure can withstand 10 N loads. When the rib inclination angle is 0°, the maximum displacement generated by the

finger is about 11.1 mm, and there is no layer blocking phenomenon. When the rib inclination angle is 30°, the maximum displacement of the finger reaches the lowest 7.8 mm due to the obvious layer blocking effect. The error with the simulation result is no more than ±0.2 mm, which verifies the correctness of the above simulation.

5.3. Clamping Experiment

5.3.1. Static Clamping Experiment. The end-effector grabs the tomato, and the tension gauge is connected to the tomato. Simulate the working state of the robot pulling tomatoes when picking, and test whether the gripping force of the end-effector meets the requirements. During the test, the average reading of the tension gauge was around 7 N, as shown in Figure 16(a). It is verified that the flexible end-effector can withstand a tensile force of 7 N, the load is more than 2 times its own weight, and the performance is excellent, which meets the needs of picking operations.

The tomato was divided into three intervals of 65~75 mm, 75~85 mm, and 85~95 mm for the clamping

(a) (b)

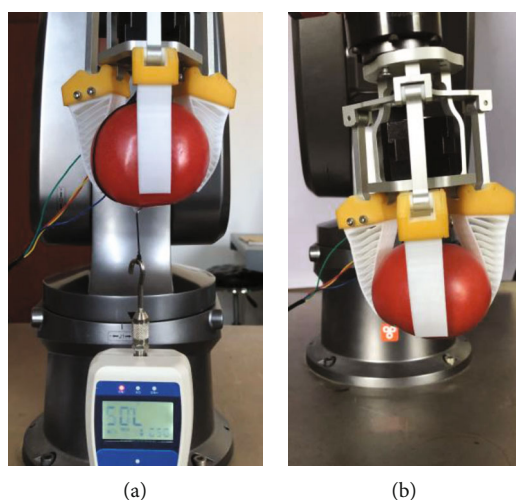FIGURE 15: Fingers bear 10 N load: (a) six-rib finger structure; (b) ten-rib finger structure.

(a) (b)

FIGURE 16: Static clamping experiment: (a) force test; (b) stability test.

TABLE 4: Experimental results.

Tomato size (mm)	Maximum clamping force (N)	Average coverage (%)	Effective grab rate (%)
65~75	5.61	32.5	100
75~85	6.84	26.9	100
85~95	7.86	23.6	100

experiment. 10 tomatoes were selected in each interval to verify the versatility of the end-effector for tomato grasping. The end-effector held the tomato for 30 seconds, and the peel was not damaged after release, which was counted as a valid grab. Record each thin film piezoelectric sensor reading as shown in Figure 16(b). Calculate the approximate surface area S_1 ($S_1 = \pi R^2$) of the tomato with the lateral diameter R, and record the gripping range of the fingers during the gripping process. Calculate the surface utilization area S_2 of the finger fins. Finally, calculate the average coverage ρ ($\rho = S_2/S_1$) of the fingers on tomatoes of different sizes.

The experimental results are shown in Table 4. For tomatoes with larger diameter sizes, the coverage is over 20%. For tomatoes with smaller diameters, the coverage is over 30%. The average clamping force is less than 8 N, and the effective grasping rate is 100%. Therefore, the flexible end-effector can achieve stable and nondestructive grasping of tomatoes with diameters ranging from 65 to 95 mm, which proves the rationality of the improved finger design.

5.3.2. Dynamic Clamping Experiment. Typically, after the end-effector holds the tomato, a dynamic transport process takes place. Therefore, 20 tomatoes were randomly selected to simulate the working environment of the sorting robot for testing. The test steps are shown in Figure 17. The end-effector moves to the designated position to hold the tomato, moves up 10 cm vertically, moves 30 cm horizontally, and finally moves down 10 cm vertically and places it on the workbench. Tomatoes did not fall off, and the surface was not damaged during this process, which was counted as an effective sorting. The experimental results showed that the tomato did not fall off, and the tomato did not suffer from damage to the clamping. It is proved that the flexible end-effector has superior performance and is fully suitable for tomato picking and sorting.

According to the real picking scene, the tomato picking experiment was carried out on the end-effector. A comparative experiment is carried out on the two most common three-finger end-effectors. As shown in the picking experiment in Figure 18(a), the fingers of the pneumatic soft end-effector are made of silicone. In the inflated state, the inner finger air bag expands, and the finger size increases. If there is a slight angle deviation, the soft fingertips will easily touch the tomato. The fingers will bend inward, causing the grasp to fail. In the tensile test, the tensile force meter reading is only 4.83 N. The clamping force is small, which causes the tomatoes to slip easily, and the picking success rate is low. The rigid end-effector shown in Figure 18(b) has a larger clamping force. However, due to the immature research on the control strategy of the current end-effector, there is no closed-loop control between the motor drive and the sensor feedback, which often leads to the occurrence

FIGURE 17: Dynamic clamping experiment.
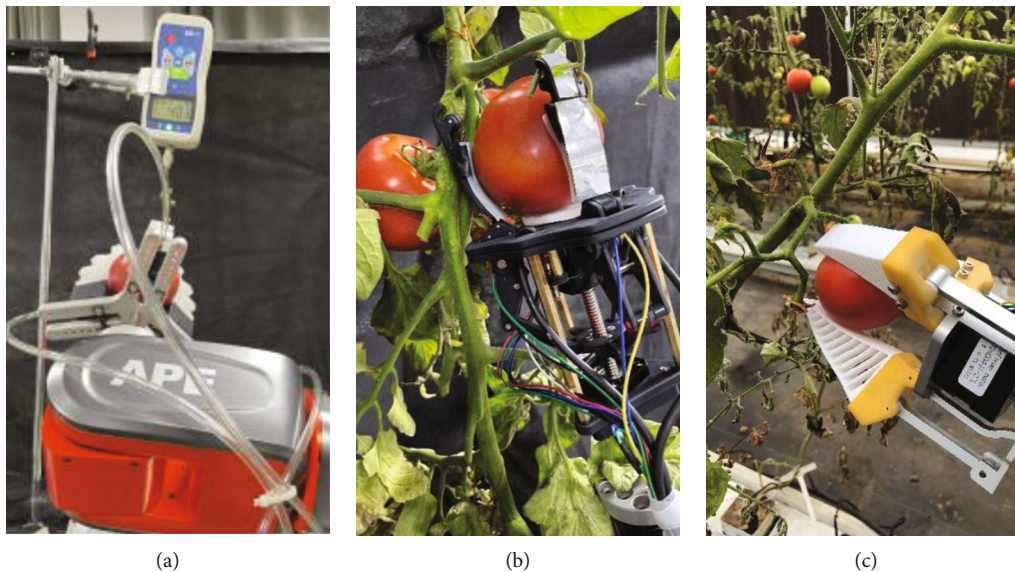
(a)	(b)	(c)

FIGURE 18: Actual picking experiment: (a) flexible pneumatic end-effector; (b) rigid end-effector; (c) the end-effector designed in this paper.

of tomato damage by clamping. Comparing with the existing products, it is found that the end-effector fixing component designed in this paper and the finger structure and size design optimized by simulation and experiment are more reasonable. As shown in Figure 18(c), while ensuring nondestructive grasping, the grasping force is large. It has strong adaptability for complex tomato picking scenes.

6. Conclusion

(1) A flexible underactuated end-effector suitable for tomato picking and sorting was designed according to the brittleness and particularity of tomato, combined with the principle of bionics. Mainly for the harvest of tomato with a diameter of 65~95 mm and a mass of not more than 500 g.

(2) Based on the experiment of tomato physical properties, it was obtained that the lateral diameter of the

tomato ranged from 66.4 to 92.7 mm, the height of the lateral diameter ranged from 35.1 to 62.7 mm, and the maximum nondestructive clamping force was 8 N. Combined with the bionics principle of the FRE structure, the flexible finger structure was designed, and the finite element analysis of the finger was carried out. The optimal structural parameters of the finger are obtained: the number of ribs is 10, the thickness of the ribs is 0.6 mm, and the inclination angle of the ribs is 30°.

(3) The single-finger experiment was performed on the end-effector, and the grid-like structure was obtained as the most suitable surface feature structure of the finger. The finger force deformation experiment verifies the correctness of the simulation results and the rationality of the finger design. The static clamping experiment of the end-effector verifies that the flexible end can withstand a tensile force of 7 N, and the

load exceeds 2 times its own weight. The coverage rate of tomato is 23.6~32.5%, and the effective clamping rate is 100%. It has strong versatility and meets the requirements of picking operations. The results of dynamic clamping experiments proved that the end-effector can hold and transport tomatoes of different sizes stably and nondestructively. It has strong protection and meets the requirements of sorting operations. Compared with the existing two common end-effectors, that is found that the end-effector designed in this paper has a large grasping force while ensuring nondestructive grasping. It has strong adaptability for complex tomato picking scenarios and provides solutions for the design and application of tomato picking and sorting robot end-effectors.

(4) In the future research, we will focus on the research of tomato visual recognition and localization and picking strategies. Solve the problems that still exist in tomato picking, such as the tomato recognition rate is not up to standard, the picking strategy is not perfect, and the picking sequence and pose are unreasonable. The designed flexible manipulator was put into a large-scale tomatoes picking scene for application research.

Data Availability

The data used to support the findings of this study are available from the corresponding author upon request.

Conflicts of Interest

The authors declare no conflict of interest.

Acknowledgments

References

[1] R. Gupta, S. Y. Kwon, and S. T. Kim, "An insight into the tomato spotted wilt virus (TSWV), tomato and thrips interaction," *Plant Biotechnology Reports*, vol. 12, no. 3, pp. 157–163, 2018.

[2] Z. Xin, Y. Cui, X. Yang, L. Kong, and Q. Lin, "Research progress on the status quo of the global vegetable industry and the development path of vegetable breeding in China," *Molecular Plant Breeding*, vol. 20, no. 9, pp. 3122–3132, 2022.

[3] A. Bechar, S. Yosef, S. Netanyahu, and Y. Edan, "Improvement of work methods in tomato greenhouses using simulation," *Transactions of the ASABE (American Society of Agricultural and Biological Engineers)*, vol. 50, no. 2, pp. 331–338, 2007.

[4] N. Ni, X. Wang, S. Wang, S. Wang, Z. Yao, and Y. Ma, "Structure Design and Image Recognition Research of a Picking Device on the Apple Picking Robot," *6th IFAC Conference on Bio-Robotics*, vol. 51, pp. 489–494, 2018.

[5] A. I. Setiawan, T. Furukawa, and A. Preston, *A low-cost gripper for an apple picking robot, Robotics and Automation*, Proceedings. ICRA '04.2004 IEEE International Conference on. IEEE, 2004.

[6] B. Wei, J. He, Y. Shi, G. Jiang, X. Zhang, and Y. Ma, "Design and experiment of underactuated citrus end-effector," *Transactions of the Chinese Society for Agricultural Machinery*, vol. 52, no. 10, pp. 120–128, 2021.

[7] L. van Herck, P. Kurtser, L. Wittemans, and Y. Edan, "Crop design for improved robotic harvesting: a case study of sweet pepper harvesting," *Biosystems Engineering*, vol. 192, pp. 294–308, 2020.

[8] T. Fujinaga, S. Yasukawa, and K. Ishii, *Development and Evaluation of a Tomato Fruit Suction Cutting Device*, 2021 IEEE/SICE International Symposium on System Integration (SII), 2021.

[9] Zhipeng Li, *Design and Research of Navel Orange Picking Robot, [Ph.D. thesis]*, Nanchang University, 2020.

[10] H. Yaguchi, K. Nagahama, T. Hasegawa, and M. Inaba, *Development of an Autonomous Tomato Harvesting Robot with Rotational Plucking Gripper*, 2016 IEEE/RSJ International Conference on Intelligent Robots and Systems (IROS), 2016.

[11] J. Lee, W. Han, E. Kim, I. Choi, and S. Yang, *A Stiffness-Controlled Robotic Palm Based on a Granular Jamming Mechanism*, 2020 17th International Conference on Ubiquitous Robots (UR), 2020.

[12] A. Alsakarneh, S. Alnaqbi, M. Alkaabi et al., "Experimental analysis of the holding-force of the jamming grippers," *Advances in Science and Engineering Technology International Conferences (ASET)*, vol. 2018, pp. 1–3, 2018.

[13] Q. Ge, A. H. Sakhaei, H. Lee, C. K. Dunn, N. X. Fang, and M. L. Dunn, "Multimaterial 4D printing with tailorable shape memory polymers," *Scientific Reports*, vol. 6, no. 1, p. 31110, 2016.

[14] Y. Miyahara and R. Kato, *Development of Thin Vibration Sheets Using a Shape Memory Alloy Actuator for the Tactile Feedback of Myoelectric Prosthetic Hands*, 2021 43rd Annual International Conference of the IEEE Engineering in Medicine & Biology Society (EMBC), 2021.

[15] M. Zhu, Y. Mori, T. Wakayama, A. Wada, and S. Kawamura, "A fully multi-material three-dimensional printed soft gripper with variable stiffness for robust grasping," *Soft Robotics*, vol. 6, no. 4, pp. 507–519, 2019.

[16] Z. Wang and S. Hirai, "Chamber dimension optimization of a bellow-type soft actuator for food material handling," *IEEE International Conference on Soft Robotics (Robo Soft)*, vol. 2018, pp. 382–387, 2018.

[17] K. Zhou, L. Xia, J. Liu, M. Qian, and J. Pi, "Design of a flexible end-effector based on characteristics of tomatoes," *International Journal of Agricultural and Biological Engineering*, vol. 15, no. 2, pp. 13–24, 2022.

[18] C. Jaren, S. Arazuri, I. Arana, N. Arias, P. Riga, and B. Epalza, "Detection of mealiness in tomato by textural analysis," *Acta Horticulturae*, vol. 934, pp. 1135–1140, 2012.

[19] S. K. Min, L. M. Duizer, and A. Grygorczyk, "Application of a texture analyzer friction rig to evaluate complex texture attributes in apples," *Postharvest Biology and Technology*, vol. 186, article 111820, 2022.

[20] Z. Li, J. Liu, and P. Li, "Relationship between mechanical properties and mechanical damage of tomato in robot picking,"

Agricultural Industry Journal of Engineering, vol. 26, no. 5, pp. 112–116, 2010.

[21] M. H. Ali, A. Zhanabayev, S. Khamzhin, and K. Mussin, *Biologically Inspired Gripper Based on the Fin Ray Effect*, 2019 5th International Conference on Control, Automation and Robotics (ICCAR), 2019.

[22] J. H. Shin, J. G. Park, D. I. Kim, and H. S. Yoon, "A universal soft gripper with the optimized fin ray finger," *International Journal of Precision Engineering and Manufacturing-Green Technology*, vol. 8, no. 3, pp. 889–899, 2021.

[23] W. Crooks, S. Rozen-Levy, B. Trimmer, C. Rogers, and W. Messner, "Passive gripper inspired by Manduca sexta and the Fin Ray® Effect," *International Journal of Advanced Robotic Systems*, vol. 14, no. 4, p. 172988141772115, 2017.

[24] Y. A. Lei, *Flexible Mechanical Claw*, CN214136081U, Guangdong Province, 2021.

[25] C. Emminger, U. D. Çakmak, R. Preuer, I. Graz, and Z. Major, "Hyperelastic material parameter determination and numerical study of TPU and PDMS dampers," *Materials*, vol. 14, no. 24, p. 7639, 2021.